Contents lists available at ScienceDirect

Scripta Materialia
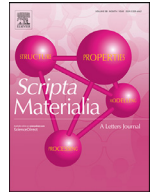
A high-strength heat-resistant Al−5.7Ni eutectic alloy with spherical Al₃Ni nano-particles by selective laser melting

Junwang Deng[a], Chao Chen[a,*], Xiaochun Liu[b,*], Yunping Li[a], Kechao Zhou[a], Shengmin Guo[c]

[a] *State Key Laboratory of Powder Metallurgy, Central South University, Changsha 410083, China*
[b] *Institute of Metals, College of Materials Science and Engineering, Changsha University of Science & Technology, Changsha 410004, China*
[c] *Department of Mechanical & Industrial Engineering, Louisiana State University, Baton Rouge, LA 70803, United States*

ARTICLE INFO

ABSTRACT

Traditional high-strength wrought aluminum alloys are sensitive to cracks in additive manufacturing (AM) while the eutectic aluminum alloys can be reliably printed. To explore a high-strength heat-resistant aluminum alloys by AM, in this paper, we proposed to retard the solidification range by using an Al−5.7Ni alloy, thus alleviate crack formation tendency. The AM parts of this alloy was featured by uniformly distributed spherical Al₃Ni nano-particles with an average size of ~33 nm, showing a novel coherent crystallographic relationship with the matrix, $<110>_{Al}//<113>_{Al3Ni}$ and $\{111\}_{Al}//\{211\}_{Al3Ni}$. Excellent mechanical property was achieved in this crack-free alloy with tensile strength of 410 MPa at room temperature and 140 MPa at 300°C, mainly attributed to the dispersion strengthening from the Al₃Ni nano-particles with superior thermal stability.

Aluminum alloys have been widely used in aerospace, spaceflight, military equipment, shipbuilding and automotive industry owing to their light weight, comparatively high specific strength, and excellent corrosion resistance [1]. Selective Laser Melting (SLM) based additive manufacturing (AM) can easily achieve the fabrication of hollowed, porous or grid structures, thus provides an rapid manufacturing method for making complex aluminum alloy components, such as box beam, thin wall and internal flow channels [2]. However, due to the intrinsically high reflectivity, high thermal conductivity, and low laser absorptivity with Al powders, Al alloy AM parts have the tendency of forming defects, such as pores and cracks in the SLM process [3]. Traditional high strength aluminum alloys such as Al2024 [4], Al2618 [5] and Al7075 [6] have a high cracking tendency during the SLM AM process. Based on the authors' prior study on Al2124 [7], it was very challenging to eliminate cracks by adjusting process parameters and scanning strategies. Crack formation limits the application of traditional high strength Al alloys in AM.

One main cause of crack during Al alloy solidification process is the large freezing range [8]. The hot cracking tendency is severer in the SLM process, due to the high cooling rates and multiple thermal cycles. Eutectic aluminum alloy (EAA) has a small freezing range duo to the overlapping liquidus and solidus temper-

atures. EAA is generally used for manufacturing parts of complex shape, which requires a good flowability and low hot crack tendency. The microstructures of EAA made by a traditional process such as casting may be lamellar or rod-like, with thick eutectic structure and large grains [9]. Al alloys with eutectic components, such as AlSi12 and AlSi10Mg, have an intrinsically small freezing range, and have been successfully applied with SLM method [10-11]. However, Al−Si alloy parts will sharply lose strength at above 200°C and cannot meet the requirements for many engineering applications, such as engine cylinder head or valve filter [12]. For elevated temperature applications, Al-Al₃Ni eutectic alloy is a promising candidate to replace Al−Si alloys due to its higher eutectic temperature of ~640°C (compared to 577°C for Al−Si) and excellent thermal properties up to 500°C [13]. Al−Ni eutectic alloy has also been reported to have an increased strength under a high cooling rate [14].

In this work, an Al−5.7Ni eutectic alloy is examined for the suitability of producing high-strength crack-free AM parts. With inherently high cooling rate (~10⁶ K/s) [15], SLM process is expected to produce fine grains and fine eutectic structures, which are generally favorable for good mechanical performance. The mechanism for high-strength Al−5.7Ni AM parts is examined by microstructure characterizations and confirmed by tensile property measurements under a wide temperature range.

To prepare Al−5.7Ni AM samples, spherical shaped Al−5.7Ni pre-alloy powders (gas atomized) were used. SLM process was carried out using a FS271 machine equipped with a Gaussian beam

---

* Corresponding authors.
E-mail addresses: pkhqchenchao@126.com (C. Chen), xcliu@csust.edu.cn (X. Liu).
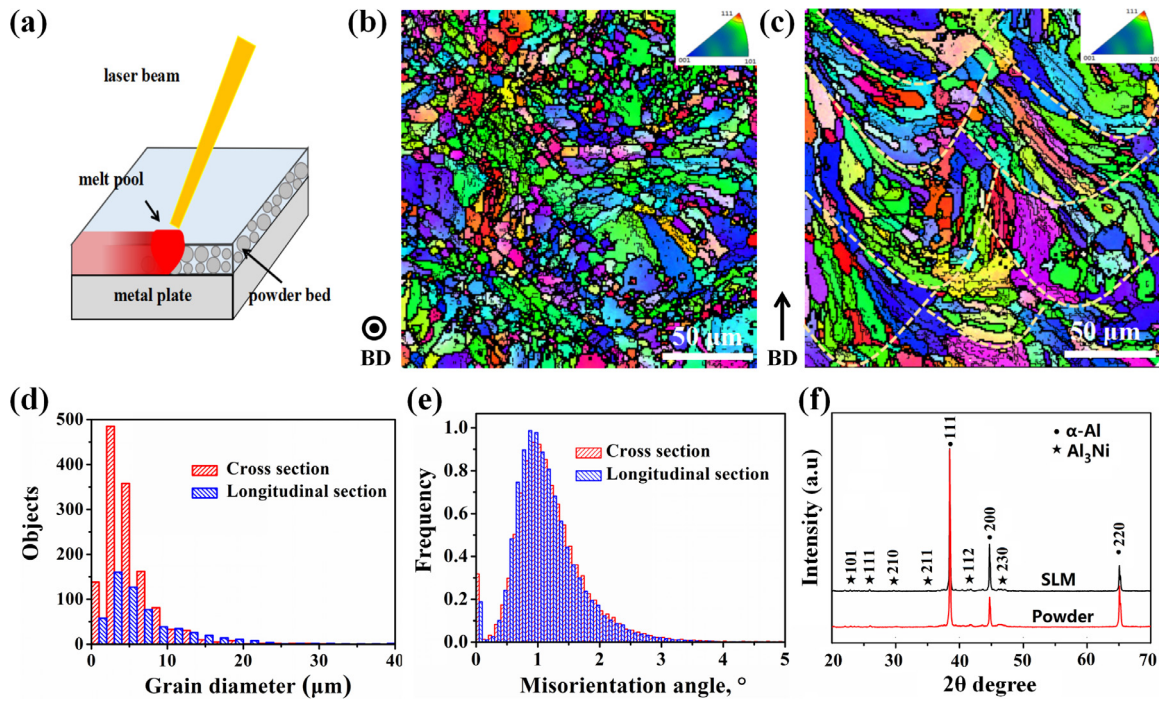
Fig. 1. (a) Schematic for SLM AM process, (b) cross section and (c) longitudinal section EBSD orientation map, (d) grain size distributions, and (e) misorientation angle distribution of Al−5.7Ni AM sample, (f) X-ray diffraction patterns of Al−5.7Ni powder and the AM samples.

fiber laser. After conducting an extensive SLM process optimization, the authors selected laser power 350 W, scanning speed 1500 mm/s for Al−5.7Ni. Tensile testing specimens were cut out from the as-built cuboids, using a wire EDM machine. The orientations of the tensile specimens are shown in Fig. S1. The cylindrical shaped tensile specimens had a total length of 51 mm, with a radius of curvature of 4 mm. The gauge section diameter was 3 mm, and the gauge length was 20 mm. The tests were performed using an Instron 3369 mechanical testing machine at 25°C, 200°C, 250°C and 300°C, respectively. For high temperature tests at 200°C, 250°C and 300°C, the samples were maintained at the pre-defined temperature for at least 10 min before testing so that homogenous temperature was achieved in the specimen. The static tensile tests were conducted under 1 mm/min. Three tensile specimens were used under each test condition. Microstructures were examined using Optical microscopy (OM, MeF3A, Leica, Germany), scanning electron microscope (SEM, JSM-6360LV), electron backscatter diffraction (EBSD, FEI, HELIOS Nano Lab 600i, with a scanning step of 1 μm), and transmission electron microscopy (TEM, FEI, Tecnai G2 F20) respectively. The elemental distribution maps of interested regions were analyzed by energy disperse spectroscopy (EDS). Polishing of the samples was accomplished on a RL-I twin-jet electropolishing device for 20 s at 15 V in corrosive liquid at −25°C. TEM specimens were prepared using Focused Ion Beam (FIB, FEI Helios Nanolab 600i). Phases of the AM samples were identified by X-ray diffraction (XRD) on a Bruker Advance D8 Discover 2500 machine over a 2θ range between 20° and 70° at a scanning rate of 0.33° min^{-1} and a wavelength of 0.15406 nm (Cu-Kα1).

The relative density of the Al−5.7Ni AM sample is 99.85%, with a few spherical shaped micro pores but crack free (Fig. S2). The EBSD maps, Fig. 1b and Fig. 1c, show the grain orientation and size distribution observed from the cross section and longitudinal section, respectively. For grain morphologies, based on the EBSD maps, we can observe equiaxed grains from the cross section and columnar grains distributed along the melt pool temperature gradient directions from the longitudinal section. The grain size distribution mainly ranges from 2~10μm. As shown in Fig. 1d, the av-

erage grain diameters of cross section and longitudinal section are 5.1μm and 7.1μm respectively. Fig. 1e shows the misorientation angle distribution of the AM sample. It is noteworthy that there exists no noticeable difference of misorientation angle between the cross section and the longitudinal section. The misorientation angle is small (0~5°) and the fraction of the low-angle grain boundaries (LAGBs) is determined to be above 90.0% (Fig. S3). A high fraction of LAGBs is beneficial to improve the strength of the parts. Fig. 1f shows both XRD patterns of the powder and the AM sample which illustrate that the main phases are α-Al and Al$_3$Ni. The detected α-Al peaks are slightly shifted to a higher angle compared to the standard diffraction peaks of Al (01-089-4037), which is attributed to the excess solid solubility of Ni in the α-Al matrix. Due to the high cooling rate of the SLM and gas atomization process, supersaturated solid solution forms [16].

To explore the mechanism of why Al−5.7Ni alloy is SLM friendly and with a high-strength, TEM analysis was performed, Fig. 2. Significant amount of spherical nano-particles are found distributing evenly in the SLM Al−5.7Ni parts, Fig. 2a. According to Al−Ni phase diagram and the XRD analysis in Fig. 1f, these spherical nano-particles are Al$_3$Ni phases. EDS surface scanning result in Fig. 2c shows that the red area is high in Al concentration and the green area is high in Ni concentration. The Ni enrichment area is in corresponding to the location of the nano-particles in Fig. 2b. EDS line scanning shows that atomic ratio of Al and Ni in those nano-particles are about 3:1, which proofs that the nano-particles are Al$_3$Ni. The average size of the spherical nano-particles is about 32.6 nm calculated by Image-Pro Plus with ten HAADF images such as Fig. 2b. Al$_3$Ni has high hardness and good thermal stability [17]. Based on the microstructure characterization of both layer-by-layer deposited part and the single molten track, it is inferred that nano-sized Al$_3$Ni forms directly from the liquid phase during the solidification stage of the SLM process. Neither grain boundary Al$_3$Ni particles nor precipitation-free zones is observed in the SLM Al−5.7Ni alloy (Figs. S4 and S5). The fine, spherical and stabilized nano-particles are coherent with the matrix and uniformly dispersed in aluminum matrix.
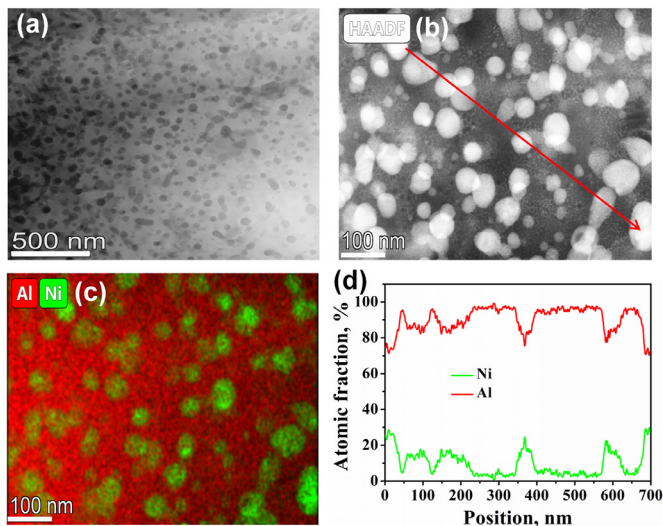
Fig. 2. (a) TEM bright-field image showing the morphology and distribution of nano-particles. (b) HAADF image of Al−5.7Ni SLM sample, (c) surface scanning and (d) line scanning of element distribution in (b) respectively.
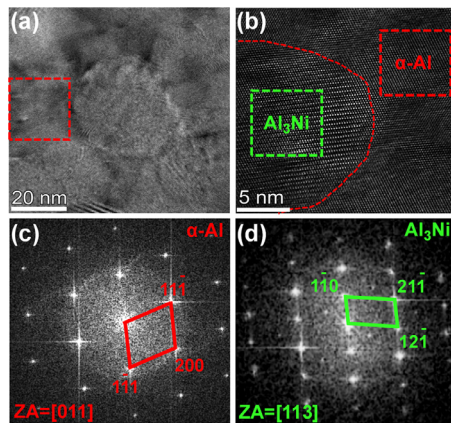

Fig. 3. (a) HRTEM image showing the phase relationship between α-Al and Al$_3$Ni, (b) the Inverse Fourier Transform of the region in the red dotted square on (a), (c) and (d) Fourier Transform diffraction spot of the regions in red and green dotted square on (b) respectively.

The maximum solubility of Ni in Al is ~0.24% mass fraction under equilibrium and ambient condition [18]. With increase of cooling rate, much more solute can be trapped, due to the high solubility of nickel in aluminum at high temperatures. At a high cooling rate, the solid solubility of Ni in aluminum could reach 8% mass fraction [19]. The spectrum analysis of the Ni average content in Al matrix is about 3.55% mass fraction. The high content of nickel in aluminum would result in supersaturated solid solutions in as-built SLM parts. In addition to Al$_3$Ni nano-particle dispersion strengthening, this supersaturated solid solution will also play a very important role in strengthening the mechanical properties of the alloy.

Fig. 3a shows the phase compositions for both spherical nano-particle and the matrix. Fig. 3b is the inverse Fourier transformed area inside the red dotted square of Fig. 3a. Fourier transform again, the diffraction patterns in Fig. 3c and Fig. 3d illustrate novel coherent Berger vector relationship (BR, $<110>_{Al}//<113>_{Al3Ni}$ and $\{111\}_{Al}//\{211\}_{Al3Ni}$) for the matrix α and the spherical nano-particle, which like superlattice structures. According to measurement, the actual distances of $\{11\bar{1}\}$ and $\{200\}$ of α-Al are 2.28 Å and 1.97 Å, while the corresponding distances in PDF CARDS of aluminum matrix are 2.34 Å and 2.02 Å respectively. Therefore, the supersaturated solid solution of Ni in Al−Ni alloy is proved again

by the decrease of crystal plane distances. The lattice constant of Al would be distorted with Ni atoms trapped in the crystal structure of Al under the condition of fast cooling non-equilibrium solidification. Both the dispersion distribution of metastable Al$_3$Ni nano-particles with complete coherence and the supersaturated solid solution would improve the mechanical properties of the alloy.

The tensile properties of SLM Al−5.7Ni samples at different temperatures are shown in Fig. 4. The horizontal SLM Al−5.7Ni shows ultimate tensile strength (UTS) of 407 MPa, yield strength (YS) of 278 MPa, and elongation (El) of 9.5% at room temperature, respectively. The tensile properties of SLM Al−5.7Ni alloy are significantly higher than those of AlSi12 [20] and AlSi10Mg [21] prepared by SLM. The considerable mechanical properties can be ascribed to the fine grains, spherical Al$_3$Ni nano-particles, supersaturated solid solution and high-density dislocations in the as-fabricated Al−5.7Ni (Fig. S6). The fast-cooling microstructure leads to various strengthening mechanisms including grain boundary strengthening, dispersion strengthening, solid solution strengthening, and dislocation strengthening. The contribution of grain boundary strengthening and dispersion strengthening to yield strength are estimated to be 59.1 MPa and 146.2 MPa, respectively (supplementary materials). As shown in Fig. 1c, microstructural anisotropy exists in SLM Al−5.7Ni alloy parts as evidenced by the columnar grains formed along the thermal gradient direction. However, the impact of anisotropy to the mechanical properties is relatively small. For example, the UTS of horizontal samples and vertical samples are 407 MPa and 433 MPa, respectively (Fig S7).

The SLM Al−5.7Ni also maintains high strength at elevated temperatures. The SLM Al−5.7Ni alloy can maintain both high UTS and YS at elevated temperature. Even at 300°C, the UTS is still above 140 MPa, which is much higher than that of SLM Al10Si0.5Mg alloy with YS ~100 MPa [22]. Due to the rapidly coarsening of Si at elevated temperatures, it was reported that the UTS of SLM AlSi12CuMgNi alloy at 300°C was only 77 MPa [23]. The high strength of Al−5.7Ni at elevated temperature is mainly attributed to the low diffusion coefficient of Ni in the aluminum matrix ($d_{Ni/Al}$=2.7 × 10^{-17} m^2/s) at the temperature of 300°C which is much lower than that of Si ($d_{Si/Al}$=2.6 × 10^{-16} m^2/s) [24]. Table 1 lists tensile properties of Al−Ni eutectic alloys at various test temperatures prepared by different methods. The morphology of Al$_3$Ni is rod-like, fibrous and lamella by cast in mold, fine particle shape by cold rolling, and nano spherical particle shape in this work. Those nano spherical Al$_3$Ni particles are the main reason for the high-strength Al−5.7Ni alloy AM parts. For comparison, the tensile strength of Al−Ni eutectic alloy SLM parts are higher than traditional casting and cold rolling counterparts at room temperature, 250°C, and 300°C, Table 1. Low diffusion rate enables spherical nano-particles Al$_3$Ni to have excellent heat resistance and maintain good strengthening effect. As a result, the tensile properties of samples manufactured by SLM at elevated temperatures are still better than those of Al−Ni eutectic alloys manufactured by traditional methods.

Up to now, there are very limited commercially available high-strength Al alloy materials for SLM. In order to develop a high strength Al alloy, the authors selected Al−5.7Ni with narrow freezing range and small crack tendency. This alloy was demonstrated successfully for SLM over a wide processing window without cracking. Under the influence of extremely high cooling rate, more Ni solution is trapped in Al matrix, resulting in solid solution strengthening. Due to the high Ni content, a large number of spherical nano-particles Al$_3$Ni are dispersed in matrix α, producing globular eutectic structures, and leading to dispersion strengthening. For SLM Al−Ni parts, these factors result in the targeted higher tensile strength than Al−Ni parts processed by traditional methods, both at room temperature and elevated temperatures.
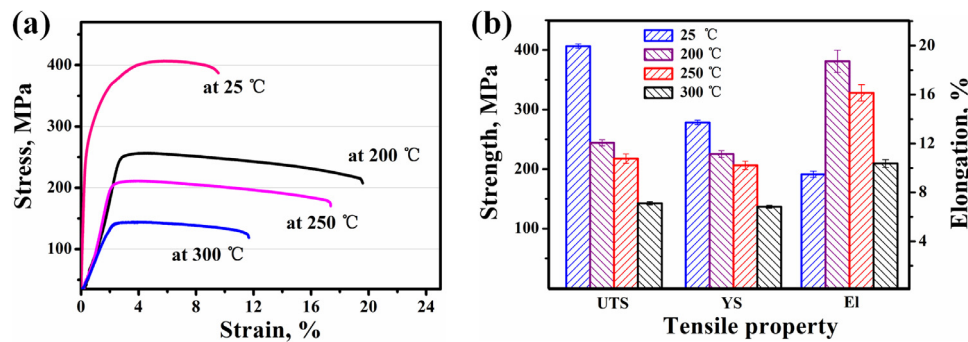
Fig. 4. (a) Tensile stress vs strain plots and (b) bar plots comparing at test temperatures of 25°C, 200°C, 250°C and 300°C for Al−5.7Ni SLM horizontal specimens respectively.

Table 1
Mechanical properties of Al−Ni eutectic alloys at various test temperatures prepared by different methods.

Alloy	Methods of fabrication	UTS, MPa	YS, MPa	El., %	Test temperature,°C	Ref.
Al−3.1 at. %Ni	Chill cast	308±14	200±9	~14	25	[12]
		132±6	120±8	~20	250	[12]
Al−6 wt. %Ni	Cold rolled	220	205	3.2	25	[25]
	Chill cast	110	89	8.6	300	[13]
Al−5.7 wt. %Ni	SLM	407±6	278±5	9.5±0.3	25	This work
	horizontal samples	218±8	206±7	16.1±0.7	250	
		143±3	137±2	10.4±0.3	300	

In summary, the authors demonstrated that using eutectic aluminum-nickel alloy (Al−5.7Ni), high-strength and crack free SLM parts can be produced. Under the high cooling rate of SLM process, the Al_3Ni phase acts as a heterogeneous nucleating agent for microstructure control. The unique microstructure of SLM Al−5.7Ni parts is the key for the observed high-strength and good elongation.

Declaration of Competing Interest

The authors confirm that there are no known conflicts of interest associated with this publication and there has been no significant financial support for this work that could have influenced its outcome.

Acknowledgments

Supplementary materials

Supplementary material associated with this article can be found, in the online version, at doi:10.1016/j.scriptamat.2021.114034.

Reference

[1] J.M Tang, Spacecraft Environment Eng., 30 (4) (2013) 352–359.
[2] D D Gu, W Meiners, K Wissenbach, R. Poprawe, Int. Mater. Rev. 57 (03) (2012) 133–164.
[3] J.L. Zhang, B. Song, Q.S. Wei, D. Bourell, Y.S. Shi, J. Mater. Sci. Technol. 35 (2019) 270–284.
[4] H. Zhang, H.H. Zhun, T. Qi, Z.H. Hu, X.Y. Zeng, Mater. Sci. Eng. A 656 (2016) 47–54.
[5] D.Palousek D.Koutny, L. Pantelejev, C. Hoeller, R. Pichler, L. Tesicky, J. Kaiser, Mater. 11 (2018) 298.
[6] W. Reschetnik, J.P. Brüggemann, M.E. Aydinöz, O. Grydin, K.P. Hoyer, G. Kullmer, H.A. Richard, in: 21st European Conference on Fracture, Pro. Stru. Int, 2016, pp. 3040–3048.
[7] J.W. Deng, C. Chen, W. Zhang, Y.P. Li, R.D Li, K.C. Zhou, Mate. 13 (2020) 4423.
[8] Z.C. Fang, Z.L. Wu, C.G. Huang, C.W. Wu, Opt. Laser Technol. 129 (2020) 106283.
[9] Y.T. Ding, S.Y Long, D.P. Jiang, Z.B. Zhu, Mater. Rep. 20 (2006) 458–459.
[10] X.P. Li, X.J. Wang, M. Saunders, A. Suvorov, L.C. Zhang, Y.J. Liu, M.H. Fang, Z.H. Huang, Acta Mater 95 (2015) 74–82.
[11] M.K. Gupta, A.K. Singl, H.S Ji, Q.H. Song, Z.Q Liu, W.T. Cai, M. Mi, N. Khanna, G.M. Krolczyk, J. Mater. Res. Technol. 9 (2020) 9506–9522.
[12] P. Pandey, S.K. Makineni, B. Gault, K. Chattopadhyay, Acta Mater 170 (2019) 205–217.
[13] C. Suwanpreecha, P. Pandee, U. Patakham, C. Limmaneevichitr, Mater. Sci. & Eng. A 709 (2018) 46–54.
[14] R. Kakitani, R.V. Reyes, A. Garcia, J.E. Spinellib, N. Cheung, J. Al, Comp 733 (2018) 59–68.
[15] J Li, X Cheng, D Liu, Q Zhang S, Z Li, B He, M Wang H, Mater. Lett. 214 (2018) 56–59.
[16] Z.H. Hu, H. Zhang, H.H Zhu, Z.X Xiao, X.J Nie, X.Y. Zeng, Mater. Sci. & Eng. A 759 (2019) 54–166.
[17] M.V. Canté, J.E. Spinelli, N. Cheung, A. Garcia, Met. Mater. Int. 16 (2010) 39–49.
[18] P. Nash, Y.Y. Pan, J. Phase Equi. 12 (1991) 105–113.
[19] Q.H. Hu, Principle of metal solidification, Second edition, Mech. Ind. Press, Beijing, 2019.
[20] J. Suryawanshi, K.G. Prashanth, S. Scudino, J. Eckert, O. Prakash, U. Ramamurty, Acta Mater 115 (2016) 285–294.
[21] L.Z. Wang, S. Wang, X.F. Hong, J. Manu. Proc. 35 (2018) 492–499.
[22] K.J. Chen, F.Y. Hun, T.S. Lui, C.L. Tsai, J. Mater. Res. Technol. 9 (4) (2020) 9242–9252.
[23] S. Yamasaki, T. Okuhira, M. Mitsuhara, H. Nakashima, J. Kusui, M. Adachi. Metals, 9 (2019) 468.
[24] Y Du, Y A Chang, B Y Huang, W P Gong, Z P Jin, H H Xu, Z H Yuan, Y Liu, Y H He, F.Y. Xie, Mater. Sci. Eng. A 363 (2003) 140–151.
[25] N.A. Belov, A.N. Alabin, D.G. Eskin, Scr. Mater. 50 (2004) 89–94.